IOP Publishing Journal of Physics: Condensed Matter
J. Phys.: Condens. Matter **28** (2016) 495801 (7pp) doi:10.1088/0953-8984/28/49/495801

Diffusion of interstitial oxygen in silicon and germanium: a hybrid functional study

Davide Colleoni and Alfredo Pasquarello

Chaire de Simulation à l'Echelle Atomique (CSEA), Ecole Polytechnique Fédérale de Lausanne (EPFL), CH-1015 Lausanne, Switzerland

E-mail: davide.colleoni@epfl.ch

Received 15 July 2016, revised 16 September 2016
Accepted for publication 20 September 2016
Published 12 October 2016

Abstract

The minimum-energy paths for the diffusion of an interstitial O atom in silicon and germanium are studied through the nudged-elastic-band method and hybrid functional calculations. The reconsideration of the diffusion of O in silicon primarily serves the purpose of validating the procedure for studying the O diffusion in germanium. Our calculations show that the minimum energy path goes through an asymmetric transition state in both silicon and germanium. The stability of these transition states is found to be enhanced by the generation of unpaired electrons in the highest occupied single-particle states. Calculated energy barriers are 2.54 and 2.14 eV for Si and Ge, in very good agreement with corresponding experimental values of 2.53 and 2.08 eV, respectively.

Keywords: oxygen diffusion, silicon, germanium, hybrid functional calculation, nudged-elastic-band

(Some figures may appear in colour only in the online journal)

Introduction

The microelectronic industry has long relied on silicon and its interface with silica. However, the continuous scaling of microelectronic devices has reached the physical limit for these materials. Substrate materials, among which strained Si and high-mobility semiconductors such as Ge, are currently under scrutiny to allow further device scaling and to improve their performances [1–4]. The technological need for growing defect-free interfaces has driven many investigations making of the silicon oxidation reaction one of the most studied atomistic processes [5–8]. The consideration of alternative substrate materials has not diminished the interest in oxygen-related processes. In any circumstance, the realization of a microelectronic device still implies the formation of a semiconductor/oxide interface through the exposure of the semiconductor to oxygen or through the deposition of oxides. In germanium, this process is shown to introduce a large number of interfacial defects causing detrimental effects on the operation of the device [2, 4]. In particular, the low thermal stability of its natural oxide (GeO_2) represents the main obstacle to the widespread use of this material [4, 9]. The Ge/GeO_2 interface is characterized by the presence of amorphous substoichiometric oxides which can trap the charge carriers hampering the proper operation of the device. The role of oxygen in the formation of these superficial states has been previously highlighted and involves the formation of valence alternation pairs [10] or of complexes acting as thermal donors [11]. The general understanding of the behavior of oxygen in semiconductors thus still remains an important research topic.

However, despite the large efforts deployed by the research community, the mechanism underlying the diffusion of an isolated oxygen atom in bulk Si has long remained poorly understood, with simulation studies yielding a variety of different paths and energy barriers [12–20]. Only recently, the O diffusion process in silicon has been clarified by reconciling the results of various theoretical schemes [17]. These recent developments call for a reconsideration of the description of the same process in germanium, which remains to be elucidated.

In silicon, atomic oxygen is mainly incorporated in an interstitial site bridging two regular nearest-neighbor atoms of the lattice [21]. Such an oxygen atom diffuses by hopping through adjacent interstitial sites with an experimentally well-characterized energy barrier of 2.53 eV [22–24]. This diffusion process has been the object of several atomic-scale

simulation studies leading to contradictory pictures. Early density-functional-theory calculations suggested that the O diffusion occurred through a symmetric path in which the transition state (TS) is represented by a threefold coordinated O atom, known as Y-lid configuration [18]. Energy barriers ranged between 1.8 and 2.4 eV when calculated with local or semilocal functionals [12–15, 18], and increased to 2.7 eV with hybrid functionals [14]. At variance, empirical potential calculations suggested an asymmetric diffusion path and yielded an energy barrier of 2.5 eV [16], in much better agreement with the experiment. Recently, a density-functional-theory study based on an advanced path sampling method has recovered an asymmetric minimum energy path with an energy barrier of ∼2.7 eV, bringing the various theoretical approaches in closer agreement with each other and with experiment [17].

As in silicon, O atoms in bulk germanium are incorporated as interstitial defects in the bridging site (O_b) [25]. Stress-induced dichroism experiments indicate that the isolated O_b impurity diffuses from one site to a neighboring one overcoming an energy barrier of 2.08 eV [26]. Density-functional-theory studies focusing on oxygen migration in Ge suggest that this process occurs through a symmetric path in which the transition state corresponds to the Y-lid configuration, with an activation energy ranging between 1.7 and 1.9 eV [18, 19]. However, in analogy to the case of silicon, empirical potential methods yield an asymmetric path and an energy barrier of 2.05 eV [20]. This puzzling picture calls for an accurate study as achieved for the O diffusion in silicon [17].

In this work, we study the minimum-energy path for the diffusion of interstitial O between two adjacent bond-center sites in silicon and germanium using the nudged-elastic-band model and hybrid functional calculations. In particular, for the study of O diffusion in germanium, it is critical to use a computational set-up based on hybrid functionals in order to overcome the vanishing band gap achieved with semilocal functionals. To validate suitable computational procedures and to derive accurate estimates of errors, we start our investigation by reconsidering the O diffusion step in silicon. For this system, the minimum-energy path can be achieved through the use of a semilocal density functional, as this electronic-structure scheme already achieves a nonvanishing band gap. A hybrid functional is then used *a posteriori* to improve the evaluation of the energy barrier. In particular, the O diffusion in silicon allows us to benchmark various procedures to be used in the more challenging case of germanium. For the O diffusion step in both silicon and germanium, we observe a peculiar spin effect leading to the unpairing of the electrons in the highest occupied state at the transition state. This effect stabilizes the transition state and yields a lower energy barrier. The calculated transition barriers are found to agree well with experimental estimates. This work provides convincing evidence that the critical diffusion step of O atoms in both silicon and germanium proceeds through an asymmetric minimum-energy path and that density functional calculations can quantitatively reproduce the experimental migration barrier.

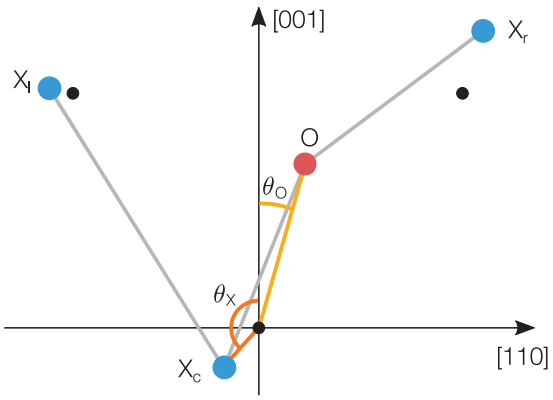

Figure 1. Schematic representation of the interstitial O defect in the bond-center site and definition of the angles θ_O of the O atom and θ_X of the central atom of the host material, as calculated along the diffusion path. The relevant atoms of the host are the central atom X_c, the atom at the left X_l, and the atom at the right X_r. The symbol X refers to either Si or Ge, depending on the material under consideration. All the atoms are in the [1 1 0] plane of the host crystal. Small black points indicate the atomic positions in the unperturbed bulk.

Modelling details and benchmark tests

Parametrization of the minimum-energy path

The diffusion of an interstitial O atom in Si and Ge occurs through a jump from a bond-center site to the adjacent one in the [1 1 0] plane of the crystal. The path can be parametrized through the angle θ_O which identifies the position of the O atom with respect to the (0 0 1) direction. As shown in figure 1, this angle is centered at the unperturbed bulk position of the central atom (X_c) taken as fixed origin, where X is either Si or Ge. Similarly, we define the angle θ_X for the central X atom. The atoms of the host at the right (X_r) and at the left (X_l) of the O defect in figure 1 are also relevant for the description of the O diffusion process. Our calculations indicate that the minimum-energy path is asymmetric. We note that the finding of an asymmetric path implies the occurrence of two paths equivalent by mirror symmetry [17].

For a symmetric diffusion path, the transition state occurs at $\theta_O = 0°$ and $\theta_X = 180°$ with both the O and X_c atoms being equidistant from the X_r and X_l atoms. We denote the configuration with these structural parameters as the Y-lid configuration [18]. To obtain the symmetric Y-lid configuration, we perform structural relaxations subject to symmetry constraints. The applied constraints allow the O atom to relax along the [0 0 1] direction, while the silicon lattice is prevented from moving by fixing the positions of a few distant Si atoms.

Computational details

The structural rearrangements go with the appearance of electronic states moving into the band gap and affecting the energetics of the migration process [17]. Thus, it is critical to well reproduce the bulk electronic properties of the host material in order to achieve an accurate description of the diffusion process. While the experimental band gap of germanium measures 0.74 eV [31], local and semilocal approximations to

density functional calculations yield metallic behavior. The closure of the band gap in such schemes prevents us from reliably studying the O diffusion step. In order to address the O diffusion in germanium, it is therefore necessary to adopt a theoretical scheme which ensures the existence of a band gap. We here rely on the hybrid functional proposed by Heyd, Scuseria, and Ernzerhof (HSE) [32]. Since the use of this functional is computationally expensive, it is important to establish a protocol to minimize the calculations which need to be carried out at the HSE level. With this aim in mind, we thus first reconsider the oxygen diffusion process in silicon.

The calculations for the O diffusion in silicon are based on the semilocal density functional introduced by Perdew, Burke, and Ernzerhof (PBE) [33]. We use a plane-wave basis set with a kinetic energy cutoff of 70 Ry together with norm-conserving pseudopotentials, as implemented in the Quantum-ESPRESSO suite of programs [34]. For the equilibrium lattice parameter and for the bulk modulus, we find 5.46 Å and 878 kbar, in good agreement with their experimental counterparts of 5.43 Å and 978 kbar [27, 28], respectively. The diffusion path is studied with the nudged-elastic-band (NEB) method [35, 36]. In light of the computational benchmarks in [17], we perform the NEB calculations with a 216-atom supercell at the PBE lattice parameter and sample the Brillouin zone at the sole Γ point. For silicon, this method yields an asymmetric transition state, which corresponds to the minimum-energy path [17]. To improve the description of the silicon band gap, we calculate the final energy barriers at the HSE level without performing additional structural relaxations. We use the HSE implementation as provided in Quantum-ESPRESSO package [37], in which the exchange potential is treated as described in [38]. In this work, we use the HSE hybrid functional in its standard implementation with parameters $\alpha = 0.25$ and $\mu = 0.11$ bohr^{-1} [32]. For a 2-atom unit cell with a converged **k**-point sampling, we thus obtain a band gap of 1.18 eV, in good agreement with the experimental value of 1.17 eV [39].

In our study of O diffusion in germanium, we use a norm-conserving pseudopotential including nonlinear core corrections that has already successfully been employed in previous studies [17, 40]. The valence wave functions are described through a plane-wave basis set defined by a kinetic energy cutoff of 70 Ry. At the PBE level, we compute bulk properties, such as the equilibrium lattice parameter and the bulk modulus, obtaining 5.76 Å and 590 kbar, respectively. The HSE functional yields a lattice parameter of 5.82 Å and a bulk modulus of 600 kbar, in fair agreement with the experimental values of 5.66 Å and 750 kbar [30]. The present results are summarized in table 1. At the HSE equilibrium lattice constant of 5.82 Å (see table 1), we achieve a band gap of 0.41 eV, which noticeably underestimates the experimental value of 0.74 eV [31]. To improve the band gap in the NEB calculations, we are confronted with two possible procedures. Following a common practice, we could adjust the fraction α of Fock exchange in the HSE functional. However, assuming a linear extrapolation based on the PBE ($\alpha = 0$) and the standard HSE ($\alpha = 0.25$) results [41], we derive that the equilibrium lattice parameter would unsatisfactorily overestimate the experimental value by ∼4%. Alternatively, we could impose a lattice constant which would yield a band gap in close agreement with experiment. For instance, fixing the Ge lattice constant to 5.76 Å, corresponding to the equilibrium PBE lattice constant, results in a HSE band gap of 0.78 eV, in close agreement with the experimental value of 0.74 eV [31]. The latter appears as a good trade-off to achieve at once a good description of both lattice parameter and band gap. In the next section, we provide estimates of the errors associated to this procedure. To make the NEB calculations affordable, we use a 64-atom supercell. The final energy barriers are then obtained with a 216-atom supercell following an embedding procedure, validated previously in the case of silicon [17]. Upon the embedding in the 216-atom supercell, all the atomic positions but those corresponding to the first and second neighbors of the O atom are further relaxed. Furthermore, in order to speed up the HSE calculations, we set the density cutoff used in the hybrid functional self-consistency cycles to 2.6 times the kinetic energy cutoff instead of the default value of 4 times. We check that this setting does not affect the total energies, the single-particle energy levels, and the electrostatic potential within 0.1 meV. Similarly, the atomic forces remain invariant within $4 \cdot 10^{-6}$ eV Å^{-1}.

Table 1. Lattice parameter (a_0), bulk modulus (B), and band energy gap (E_g) for Si and Ge calculated with PBE and HSE functionals.

	a_0 (Å)	B (kbar)	E_g (eV)
Si	5.46	878	1.18
Expt.	5.43[a]	978[b]	1.17[c]
Ge (PBE)	5.76	590	0.0
Ge (HSE)	5.82	600	0.41
Expt.	5.66[d]	750[d]	0.74[e]

[a] Weast [27]. [b] Hopcroft *et al* [28]. [c] Long [29]. [d] Madelung [30]. [e] Varshni [31]
Note: Corresponding experimental values are taken from [27–31].

Benchmark tests

We perform several benchmark tests in order to estimate the accuracy of our final energy barriers. We proceed in the same spirit as in [17], but we address a larger set of sources of error. In particular, we consider the finite-size error, the uncertainty associated to the embedding procedure, the effect of atomic relaxations performed at the hybrid functional level, the role of van-der-Waals interactions, the explicit treatment of 3*d* electrons and spin–orbit interactions, and the error associated to the adopted lattice parameter.

For the same computational set-up adopted in this work, the effect of using a finite supercell has been investigated in [17] through the Y-lid configuration of the O defect in silicon, resulting in an error estimate of ∼0.05 eV. Here, we perform a similar test for germanium. We consider the energy barrier of the Y-lid structure and perform PBE calculations in which the Brillouin zone of the supercell is sampled at the sole Γ point. The value calculated with a 216-atom cell underestimates the results obtained with a 512-atom cell by only ∼0.03 eV. This result shows that the 216-atom supercell gives a satisfactory level of convergence for the purpose of this work. We expect the finite size error to be even smaller in the HSE calculation due to the opening of the band gap.

Table 2. The angles θ_O and θ_X, the distances between O and the three nearest-neighbor atoms of the host crystal, and the distances X_c–X_l and X_c–X_r atoms, as obtained for the Y-lid configuration and the asymmetric transition state (TS).

	θ_O	θ_X	O–X_c	O–X_l	O–X_r	X_c–X_l	X_c–X_r
Si							
Asym. TS	17.9°	138.9°	1.69	1.74	2.43	2.72	3.31
Sym. TS	0.0°	180.0°	1.76	1.86	1.86	2.88	2.88
O_b	−44.8°	122.7°	1.62	3.00	1.62	2.34	3.22
Ge							
Asym. TS	20.6°	133.0°	1.83	1.85	2.35	2.90	3.24
Sym. TS	0.0°	180.0°	1.84	2.00	2.00	3.01	3.01
O_b	−29.4°	122.2°	1.77	2.90	1.77	2.46	3.36

Note: The structural parameters for the initial (and final) ground-state O_b configuration are also given. Distances are given in Å.

Table 3. Energy barriers (in eV) of the O jump in Si and Ge through symmetric (Y-lid) and asymmetric transition states (TS).

	64-atom	216-atom		
	HSE	PBE	HSE	Expt.
Si	—			
Asym. TS	—	2.18 (NEB)	2.54 (SCF)	2.53
Y-lid	—	2.19 (RSC)	2.74 (RSC)	2.53
Ge				
Asym. TS	1.69 (NEB)	—	2.14 (Emb)	2.08
Y-lid	1.77 (RSC)	—	2.25 (Emb)	2.08

Note: Various methods are used: nudged-elastic-band (NEB), relaxation subject to symmetry constraints (RSC), embedding procedure (Emb), or using PBE configurations without further relaxation (SCF). Experimental values are taken from [22–24, 26].

A supercell of 216 atoms is computationally prohibitive when used in NEB calculations with a hybrid functional. We therefore have recourse to an embedding scheme, for which we determine here the related errors. Since the study of the O diffusion is computationally less demanding in silicon than in germanium, we use our PBE results obtained for silicon to validate the embedding procedure adopted to overcome the finite-size effect in germanium. In [17], the embedding procedure applied to the Y-lid configuration has been show to introduce an error of only 0.06 eV. Here, we extend this test to include the asymmetric transition state. Using the NEB method on the full 216-atom supercell at the PBE level (*vide infra*), we obtain an energy barrier of 2.18 eV, to be compared with the value of 2.22 eV obtained from the embedding procedure in [17]. The small difference of 0.04 eV further confirms that the embedding procedure is a reliable technique to overcome finite-size effects. We will apply this procedure to the HSE calculations on germanium.

To estimate the effect associated to hybrid functional relaxations, we resort to the Y-lid configuration in silicon, for which we perform a HSE structural relaxation subject to symmetry constraints (RSC). We obtain an energy barrier of 2.74 eV (see table 3), which does not differ from the value of 2.74 eV obtained without structural relaxations at the hybrid functional level, i.e. via a self-consistent-field (SCF) HSE calculation on a structure of the Y-lid configuration relaxed at the PBE level [17]. This result provides confidence to our assumption that further relaxations at the HSE level would yield negligible effects on the energy barrier associated to the asymmetric transition state for the oxygen diffusion in silicon.

It has recently been suggested that the consideration of van-der-Waals interactions lowers the calculated migration barriers by as much as 0.2 eV [42]. In order to explicitly include van-der-Waals interactions, we consider two different schemes: the rVV10 functional proposed in [43] and the Grimme correction [44]. Application of these two schemes to the oxygen diffusion in silicon enhances the PBE energy barriers by 0.16 and 0.07 eV, respectively. The effect of van-der-Waals interactions on the barrier thus differs not only in magnitude but also in sign with respect to the results in [42]. We conclude that presently available schemes for accurately estimating the van-der-Waals effect for this transition are not consistent, but appear to differ by at most ±0.2 eV. Hence, awaiting improved schemes, we do not attempt to correct our results for the van-der-Waals effect in the following.

Given the large effect that spin–orbit interaction has on the valence band maximum in germanium, we estimate to what extent these interactions affect the calculated migration barriers. For this purpose, we consider the Y-lid configuration in a 64-atom supercell at the PBE level. A fully relativistic, ultrasoft pseudopotential with 3*d* electrons among the valence states yields an energy barrier larger by only 0.05 eV than achieved with the pseudopotential used in the NEB calculations. This calculation demonstrates that the explicit treatment of spin–orbit interactions and 3*d* electrons is small.

Finally, we estimate the error associated to the choice of lattice parameter in germanium by focusing on the Y-lid configuration. We calculate the corresponding energy barrier with the HSE hybrid functional at both the PBE and HSE lattice parameters, finding that the use of the PBE lattice constant results in an overestimation of ∼0.1 eV.

To conclude this section, we provide a global estimate of the errors which affect the present energy-barrier calculations. The energy barriers calculated for Si are affected by the sole finite-size error and correspond to an underestimation of 0.05 eV. For the energy barriers in germanium, we arrive at a global error estimate of 0.06 eV, which in part results from error cancellations. In making this estimate, we considered the use of finite-size supercells, the embedding procedure, the use of the PBE lattice parameter, and the implicit treatment of spin–orbit interactions and 3*d* electrons. Hence, we estimate that the energy barriers calculated in this work are accurate within an error of the order of ∼0.1 eV. The uncertainty associated to the role of van-der-Waals interactions has not been included in this estimate.

Oxygen diffusion in silicon

The structural parameters of the initial (and final) ground-state O_b configuration, of the Y-lid configuration, and of the asymmetric transition state in silicon are reported in table 2. In the O_b configuration, the calculated θ_O and the Si–O–Si

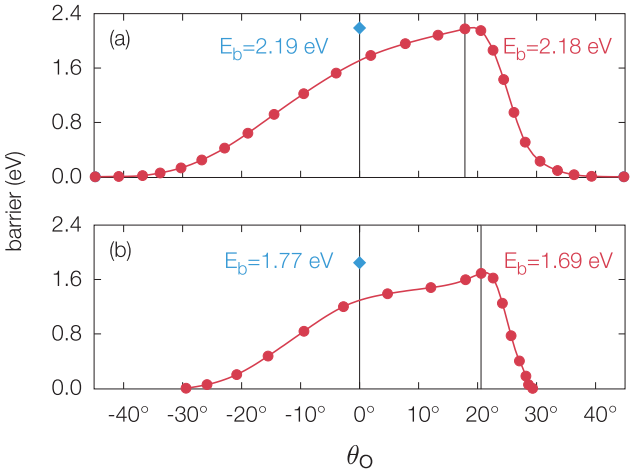

Figure 2. Minimum-energy path as a function of the oxygen angle (θ_O), as obtained with NEB calculations performed (a) for Si with a 216-atom supercell at the PBE level and (b) for Ge with a 64-atom supercell at the HSE level. The energy of the Y-lid configuration obtained through structural relaxation subject to symmetry constraints is also indicated (blue squares). Energies are referred to the corresponding O_b configurations. The vertical black lines identify the angles θ_O at which the Y-lid configuration and the asymmetric transition state occur.

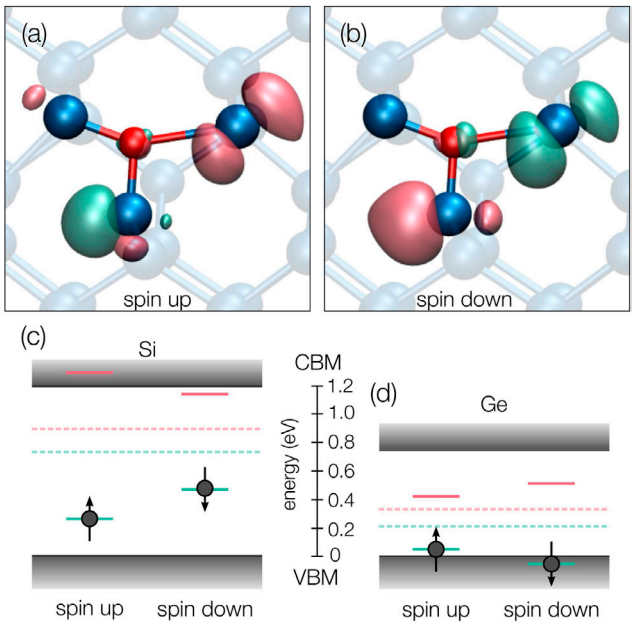

Figure 3. Charge densities of the highest occupied (light green) and of the lowest unoccupied (red) single-particle states obtained through a spin unrestricted calculation at the asymmetric transition state for Si: (a) spin up and (b) spin down components. The same picture also applies to Ge. The corresponding single-particle energy levels in the band gap are given (c) for Si and (d) for Ge. The dashed lines correspond to the energy levels of the highest occupied and the lowest unoccupied single-particle states as obtained from a spin restricted calculation.

angles agree with previous estimates achieved with a 64-atom supercell [17]. Similarly, the structural parameters of the Y-lid structure and of the asymmetric transition state show only small differences from those obtained in [17].

We investigate the asymmetric diffusion path through a NEB calculation with 24 images and a climbing image. We start from the path originally obtained for a 64-atom supercell without any climbing image and then embedded in a 216-atom supercell [17]. The transition state occurs at $\theta_O \sim 18°$ (see table 2), only slightly smaller than the value of 25° obtained with a 64-atom supercell [17]. In this state, the O atom binds to the Si_l atom, while the Si_c atom is still far from the Si_r atom. The calculated energy barrier obtained at the PBE level is 2.18 eV. Without performing further structural relaxation, we then obtain an energy barrier of 2.86 eV using the HSE functional in spin restricted calculations. This value should be compared with the result of 2.7 eV, previously obtained in a similar set-up but starting from a 64-atom supercell and using an embedding procedure [17]. The difference of ∼0.2 eV appears slightly larger than estimated in our error analysis, but can be assigned to the use of a climbing image in the present NEB calculations, which leads to an improved estimate of the energy barrier at a slightly larger value. However, the spin restricted result of 2.86 eV does not correspond to the actual energy barrier. Indeed, when a SCF spin unrestricted calculation is performed, the total energy of the transition state stabilizes by as much as 0.32 eV. This brings the calculated energy barrier to 2.54 eV (see table 3), in very close agreement with the measured activation energy of 2.53 eV [22–24].

It is of interest to analyze the origin of the observed spin polarization effect, as this has not been considered in previous works. In the spin restricted calculation, the transition state shows an electronic configuration, in which two single-particle energy levels enter the band gap, one being doubly occupied and the other one being unoccupied. These states correspond to occupied and unoccupied dangling bonds on Si_c and Si_r, respectively [17]. In the spin unrestricted calculation, we find that this description is reproduced for one spin component (see the spin up component in figure 3(a)). At variance, the picture is reversed for the other spin component (see spin down in figure 3(b)), for which the highest occupied state is localized on Si_r while the lowest unoccupied state is found on Si_c. This spin unpairing effect has been found to occur with the HSE hybrid functional, but is not seen at the PBE level. The spin unpairing suggests that the formation of the Si_c–Si_r bond is preceded by the transition of one electron from the occupied dangling bond on Si_c to the unoccupied one on Si_r. This different occupation of the single-particle states affects their energy levels, as can be seen in figure 3(c). Compared to the spin restricted result (dashed lines in figure 3(c)), the spin unrestricted calculation yields lower energy levels for the occupied states, accounting thereby for the calculated stabilization energy.

For the Y-lid configuration, we obtain an energy barrier of 2.19 and 2.74 eV at the PBE and HSE levels, respectively. At the PBE level, the energy of the Y-lid configuration is barely higher than that of the asymmetric transition state, but the difference amounts to 0.20 eV in the HSE scheme. The PBE result can be compared with a large set of previous studies at the semilocal level [13–15, 17, 18], which yield calculated barriers for the symmetric path ranging between 2.0 and 2.5 eV. Many factors contribute to this spread such as variations in supercell size, **k** point sampling, type of basis set, and adopted density functional.

With respect to previous investigations [12–15, 17, 18] the present study of O diffusion in silicon combines the NEB method with a climbing image, the use of large supercells, and energy evaluations at the hybrid functional level. In particular, a significant spin unpairing effect is revealed leading to the stabilization of the transition state by about 0.3 eV. The occurrence of an asymmetric minimum-energy path is confirmed and the calculated barrier energy is found to agree with the experimental value within an estimated residual error of 0.1 eV.

Oxygen diffusion in germanium

In the case of germanium, the ground-state O_b configuration is qualitatively similar to that found for Si. The O–Ge bond length is larger than that of O–Si by 0.15 Å, and the θ_O in germanium is smaller than in silicon by $\sim$15° (see table 2). The Ge–O–Ge angle is 142°, in agreement with previous semilocal calculations [18].

The Y-lid configuration is obtained within a 64-atom supercell through structural relaxation subject to symmetry constraints. Its structural parameters are given in table 2. The associated energy barrier is obtained with spin unrestricted calculations at the HSE level and corresponds to 1.77 eV (see figure 2). Upon embedding in a 216-atom supercell, our calculations give an energy barrier of 2.25 eV for the symmetric O diffusion path (see table 3), only slightly higher than the experimental value of 2.08 eV [26]. The present result is considerably larger than previous estimates of 1.70 eV [18] and 1.91 eV [19] obtained at the semilocal level. However, the latter studies do not only differ by the functional but also by details of the computational set-up, such as supercell size, **k**-point sampling, and type of basis set.

We then apply the NEB method using unrestricted spin calculations at the HSE level. These calculations are performed with a 64-atom supercell and 15 images, both with and without one of the images being climbing. First, we take as starting point the asymmetric path generated by rescaling the one obtained in the case of silicon [17]. The NEB calculations are initially evolved without any climbing image until the path is almost converged. The final NEB convergence steps are then carried out with one climbing image to improve the final accuracy of the result. In this way, we obtain an asymmetric minimum-energy path with an energy barrier of 1.69 eV, as shown in figure 2(b). Next, as further check, we also start the NEB calculations from a symmetric path obtained through linear interpolation of the initial and final configurations, both with and without a climbing image. These NEB calculations convert to the same asymmetric minimum-energy path shown in figure 2(b). In this minimum-energy path, the evolution of the energy barrier as a function of θ_O is overall similar to the one obtained for the O diffusion in silicon and shows a transition state at $\theta_O = 20.6°$ (see figure 2(a)). The relevant atomic distances and bond angles at the transition state are reported in table 2. The variation of the structural parameters along the asymmetric minimum-energy path are qualitatively similar to those observed for the O diffusion in Si [17]. Upon embedding in a 216-atom supercell, the energy barrier increases to 2.14 eV, bringing the theoretical result very close to the experimental value of 2.08 eV [26]. The calculated barriers and the comparison with the experimental value are summarized in table 3. The present result agrees well with a previous study based on empirical potentials [20], but differs from previous density-functional-theory calculations [18, 19] insofar the latter all failed in yielding an asymmetric minimum-energy path.

At the transition state, the highest occupied and the lowest unoccupied single-particle states correspond to dangling bonds on Ge_c and Ge_r and show the same behavior found for Si (see figures 3(a) and (b)). The corresponding energy levels with respect to the valence band edge of germanium are given in figure 3(d). As for silicon, the highest occupied states obtained in the spin unrestricted calculation (continuous lines) are lower in energy than the highest occupied level obtained in a spin restricted calculation (dashed line). It is interesting to remark that allowing for spin unpairing is critical to achieve an asymmetric minimum-energy path. Indeed, when using the NEB method with spin restricted calculations, we yield a symmetric path, in which the energy barrier is higher by $\sim$0.2 eV.

Applied to the O diffusion in germanium, our NEB calculations at the HSE level thus support an asymmetric diffusion path. The calculated energy barrier of 2.14 eV matches the experimental value of 2.08 eV within less than 0.1 eV [26].

Conclusion

We studied the minimum-energy path for the diffusion step of the interstitial O atom in Si and Ge using the NEB method and hybrid functionals. In both materials, the diffusion was found to occur through an asymmetric path. We also obtained the symmetric Y-lid configurations through relaxations subject to symmetry constraints. Their energies were found to be higher by 0.1–0.2 eV with respect to the asymmetric transition states. The calculated energy barriers for the asymmetric diffusion paths of an isolated O interstitial in Si and Ge are 2.54 and 2.14 eV, respectively. Careful validation tests indicate that these values are converged within 0.1 eV. Hence, these values are in numerical accord with the respective experimental values of 2.53 eV [22–24] and 2.08 eV [26]. This accord is particularly important as the description of these diffusion processes within a density-functional framework has long remained elusive. Nevertheless, a residual uncertainty has been highlighted concerning the role of van-der-Waals interactions, which are not described in the same way in current state-of-the-art schemes.

Acknowledgments

We thank J F Binder for providing us with the structural configurations obtained in [17]. Financial support is acknowledged from the Swiss National Science Foundation (Grant No. 200020-152799). We used computational resources of CSCS and EPFL.

References

[1] Thompson S, Sun G, Choi Y S and Nishida T 2006 *IEEE Trans. Electron Devices* **53** 1010
[2] Houssa M, Satta A, Simoen E, De Jaeger M, Meuris B, Caymax M and Heyns M 2007 *Electrical Performance of Ge Devices* (Amsterdam: Elsevier, Germanium-Based Technologies) pp 233–65
[3] Delabie A, Bellenger F, Houssa M, Conard T, Elshocht S V, Caymax M, Heyns M and Meuris M 2007 *Appl. Phys. Let.* **91** 082904
[4] Wang S K, Kita K, Lee C H, Tabata T, Nishimura T, Nagashio K and Toriumi A 2010 *J. Appl. Phys.* **108** 054104
[5] Deal B E and Grove A S 1965 *J. Appl. Phys.* **36** 3770
[6] Gusev E P, Lu H C, Gustafsson T and Garfunkel E 1995 *Phys. Rev.* B **52** 1759
[7] Pasquarello A, Hybertsen M S and Car R 1998 *Nature* **396** 58
[8] Bongiorno A and Pasquarello A 2004 *Phys. Rev.* B **70** 195312
[9] Broqvist P, Binder J F and Pasquarello A 2010 *Appl. Phys. Lett.* **97** 202908
[10] Binder J F, Broqvist P and Pasquarello A 2010 *Appl. Phys. Lett.* **97** 092903
[11] Klechko A A, Litvinov V V, Markevich V P and Murin L I 1999 *Semiconductors* **33** 1163
[12] Needels M, Joannopoulos J, Bar-Yam Y, Pantelides S and Wolfe R 1991 *Mater. Res. Symp. Proc.* **209** 103
[13] Ramamoorthy M and Pantelides S T 1996 *Phys. Rev. Lett.* **76** 267
[14] Deák P, Aradi B, Frauenheim T and Gali A 2008 *Mater. Sci. Eng.* B **154–5** 187
[15] Estreicher S K, Backlund D J, Carbogno C and Scheffler M 2011 *Angew. Chem. Int. Ed.* **50** 10221
[16] Jiang Z and Brown R A 1995 *Phys. Rev. Lett.* **74** 2046
[17] Binder J F and Pasquarello A 2014 *Phys. Rev.* B **89** 245306
[18] Coutinho J, Jones R, Briddon P R and Öberg S 2000 *Phys. Rev.* B **62** 10824
[19] Sueoka K and Vanhellemont J 2006 *Mater. Sci. Semicond. Proc.* **9** 494
[20] Gusakov V 2005 *J. Phys.: Condens. Matter* **17** S2285
[21] Hrostowski H J and Kaiser R H 1957 *Phys. Rev.* **107** 966
[22] Newman R C 2000 *J. Phys.: Condens. Matter* **12** R335
[23] Mikkelsen J C 1985 *Mater. Res. Soc. Symp. Proc.* **59** 19
[24] Watkins G. D 1996 in *Early Stages of Oxygen Precipitation in Silicon* ed R Jones (Dordrecht: Kluwer) p 1
[25] Gienger M, Glaser M and Lamann K 1993 *Solid State Commun.* **86** 285
[26] Corbett J W, McDonald R S and Watkins G D 1964 *J. Phys. Chem. Solids* **25** 873
[27] Weast R C (ed) 1988 *CRC Handbook of Chemistry and Physics* vol 69 (Boca Raton, FL: CRC Press)
[28] Hopcroft M A, Nix W D and Kenny T W 2010 *J. Microelectromech. Syst.* **19** 229
[29] Long D 1962 *J. Appl. Phys.* **33** 1682
[30] Madelung O 1992 *Physics of Group IV Elements and III-V Compounds* (Berlin: Springer)
[31] Varshni Y P 1967 *Physica* **34** 149
[32] Heyd J, Scuseria G E and Ernzerhof M 2006 *J. Chem. Phys.* **124** 219906
[33] Perdew J P, Burke K and Ernzerhof M 1996 *Phys. Rev. Lett.* **77** 3865
[34] Giannozzi P *et al* 2009 *J. Phys: Condens. Matter* **21** 395502
[35] Jónsson H, Mills G and Jacobsen K W 1998 *Classical and Quantum Dynamics in Condensed Phase Systems* ed B J Berne *et al* (Singapore: World Scientific) p 385
[36] Henkelman G, Uberuaga B P and Jónsson H 2000 *J. Chem. Phys.* **113** 9901
[37] Komsa H-P, Broqvist P and Pasquarello A 2010 *Phys. Rev.* B **81** 205118
[38] Broqvist P, Alkauskas A and Pasquarello A 2009 *Phys. Rev.* B **80** 085114
[39] Phillips J C 1962 *Phys. Rev.* **125** 1931
[40] Broqvist P, Binder J F and Pasquarello A 2009 *Appl. Phys. Let.* **94** 141911
[41] Komsa H-P and Pasquarello A 2011 *Phys. Rev.* B **84** 075207
[42] Gao W and Tkatchenko A 2013 *Phys. Rev. Lett.* **111** 045501
[43] Sabatini R, Gorni T and de Gironcoli S 2013 *Phys. Rev.* B **87** 041108
[44] Grimme S 2004 *J. Comput. Chem.* **25** 1463